

Integrating Deep Learning into CAD/CAE System: Case Study on Road Wheel Design Automation

Soyoung Yoo¹,

Sunghee Lee¹

Seongsin Kim¹

Kwang Hyeon Hwang²

Jong Ho Park²

Namwoo Kang^{1,*}

¹Department of Mechanical Systems Engineering, Sookmyung Women's University, 04310,
Seoul, Korea

²Hyundai Motor Company, 445706, Hwaseong-Si, Gyeonggi-Do, Korea

*Corresponding author: nwkang@sm.ac.kr

Abstract

Research regarding design automation that integrates artificial intelligence (AI) into computer-aided design (CAD) and computer-aided engineering (CAE) is actively being conducted. This study proposes a deep learning-based CAD/CAE framework that automatically generates three-dimensional (3D) CAD models, predicts CAE results immediately, explains the results, and verifies the reliability. The proposed framework comprises seven stages: (1) two-dimensional (2D) generative design, (2) dimensionality reduction, (3) design of experiment in latent space, (4) CAD automation, (5) CAE automation, (6) transfer learning, and (7) visualization and analysis. The proposed framework is demonstrated through a road wheel design case study and indicates that AI can be practically incorporated into end-use product design. Using this framework, it is expected that industrial designers and engineers can jointly review feasible engineering 3D CAD models created by AI and select the best design for the market in the early stages of product development. In addition, because the proposed deep learning model can predict CAE results based on 2D disc-view design, industrial designers can obtain instant feedback regarding the engineering performance of 2D concept sketches.

Keywords: Artificial Intelligence, Deep Learning, CAD, CAE, Road Wheel, Generative Design

1. Introduction

Deep learning, which is a part of artificial intelligence (AI) technology and learns meaningful patterns based on deep neural network structures from large amounts of data, demonstrates remarkable performances in various areas (LeCun et al., 2015). In recent years, the expectations for deep learning research have increased in computer-aided design (CAD) and computer-aided engineering (CAE), which are the core of new product development. Because CAD/CAE methods are based on computer technology, they can be easily combined with deep learning in comparison with other engineering fields. However, it is difficult to collect a large number of CAD models and CAE results for deep learning. Moreover, without a balanced understanding of deep learning and CAD/CAE, it is difficult to well define the problem and preprocess the data. In addition, CAD/CAE and deep learning technologies should be integrated to compensate for each other's shortcomings (Oh et al., 2019).

This paper presents an AI-based design automation process that combines deep learning with the CAD/CAE framework and validates the proposed framework through a case study pertaining to road wheel design. This allows AI to automatically create numerous feasible engineering CAD models and predict the CAE results of these models.

1.1. Deep-learning-based CAD/CAE research

Many CAD/CAE integration studies have been conducted, and considerable effort has been expended to automate the time-consuming iterative design process (i.e., design, analysis, and redesign). CAD remodeling and finite element remeshing are bottlenecks in design automation, which render it difficult to apply closed-loop-based design optimization to complex product design cases (Wang et al., 2016). Recent studies combining deep learning and CAE demonstrated the possibility of instantly predicting analysis results without finite element analysis; however, most have verified the methodology with simple engineering problems, and studies demonstrating end-use products that can be sold in the market are few.

In computer science, deep learning research using three-dimensional (3D) CAD data being actively conducted. The key to learning 3D CAD data is a pipeline design that preprocesses high-dimensional CAD data to be used as input into deep learning architectures. Based on the preprocessing technology, the three most widely used types of deep learning models are as follows: (1) voxel-based models (e.g., VoxelNet (Maturana & Scherer, 2015)), (2) point cloud-based models (e.g., PointNet (Qi et al., 2017)), and (3) view-based model (e.g., RotationNet (Kanezaki et al., 2018) and multiview convolutional neural networks (CNNs) (Su et al., 2015)). In addition, a method of learning the mesh data of the CAD model exists, i.e., MeshNet (Feng et al., 2019).

Engineering design research has focused on predicting engineering performance by learning the data obtained through CAE based on the 3D deep learning technology introduced above. Cunningham et al. (2019) conducted a study to predict the aerodynamic performance by preprocessing a 3D aircraft model into 3D point clouds and applying deep learning. Khadilkar et al. (2019) automatically generated 3D CAD models of various shapes and then sliced the models to obtain cross sections. A CNN model has been proposed to predict stresses on a cross section that occur during bottom-up 3D printing using both the cross section and 3D point cloud of the 3D model. In vehicle system design, researchers have used an autoencoder to parameterize automotive 3D mesh models, generate 3D mesh models of various shapes, and learn the computational fluid dynamics (CFD) results of models with Gaussian process regression analysis (Umetani, 2017; Umetani & Bickel, 2018).

Computer aided manufacturing (CAM) are also in progress. Williams et al. (2019) proposed a 3D CNN to estimate manufacturability by predicting the part mass, support material mass, and build time required to three-dimensionally print a CAD model. Zhang et al. (2018) conducted a study to automatically generate CAD data according to machining features, learn data through a 3D CNN, and predict machining features.

Compared with 3D designs, more studies have been performed to investigate the engineering performances of two-dimensional (2D) designs. Guo et al. (2016) proposed a CNN model that approximates a steady flow on a vehicle's side view 2D geometry, whereas Nie et al. (2020) proposed a generative model that predicts the 2D stress field of a 2D cantilever bar by learning the design space and boundary conditions.

Deep-learning-based 3D CAD/CAE research is difficult because of the following reasons. First, it is difficult to collect a large amount of 3D CAD data in the target product area; second, it is difficult to collect a large amount of CAE results to be used as labels. Therefore, to combine 3D CAE/CAE research with deep learning, an automation method should be proposed for data collection. Recently, a deep learning methodology based on physics constraints has been proposed to overcome data shortage (Sun et al., 2020); however, this approach cannot be generalized to complex product design problems associated with various physics constraints.

Owing to the recent development of *generative design*, CAD data may be automatically generated (Matejka et al., 2018). An integration of generative design and deep learning has been proposed to produce large amounts of feasible aesthetic and engineering designs (Oh et al., 2018, 2019). Similarly, a generative design technique combining deep learning and CAD/CAE was adopted in our study.

From the perspective of deep learning architecture, to build surrogate models of engineering problems, deep neural networks (DNNs) and CNN-based supervised learning are mainly used initially; however, the use of unsupervised learning (i.e., generated models) is increasing (Cheng, et al., 2020). In particular, transfer learning methods are widely used, in which dimensionality reduction is performed through unsupervised learning (Cunningham et al., 2019; Li et al., 2020). Similarly, this approach was used in this study for the proposed architecture.

1.2. Research Purpose

The purpose of this study is to propose an AI-based design automation process that incorporates deep learning into the CAD/CAE framework. The proposed framework includes (1) 2D generative design, (2) dimensionality reduction, (3) design of experiment (DOE) in latent space, (4) 3D CAD automation, (5) CAE automation, (6) transfer learning, and (7) visualization and analysis. This framework is demonstrated through a case study pertaining to road wheel design.

This framework enables one to (1) automatically generate a large number of 3D wheel CAD models that have high engineering performances, and (2) immediately predict the engineering performance based on a disc-view 2D wheel design without a 3D modeling process.

The proposed framework is expected to change the paradigm of the vehicle wheel CAD/CAE process. The existing development process is inefficient because the industrial designer creates only a small portion of the design, whereas the engineer creates a CAD/CAE model and provides feedback to the industrial designer, thereby repeating the design modification process. However, in the proposed framework, AI first generates a large amount of superior CAD models, whereas industrial designers and engineers can verify, select, and modify them. Owing to AI, designers and engineers can collaborate more efficiently.

The remainder of this paper is organized as follows. Section 2 introduces the proposed deep CAD/CAE framework. Sections 3–9 provide the details of the seven steps of the proposed framework. Section 10 presents the conclusions and future research directions.

2. Deep CAD/CAE Framework

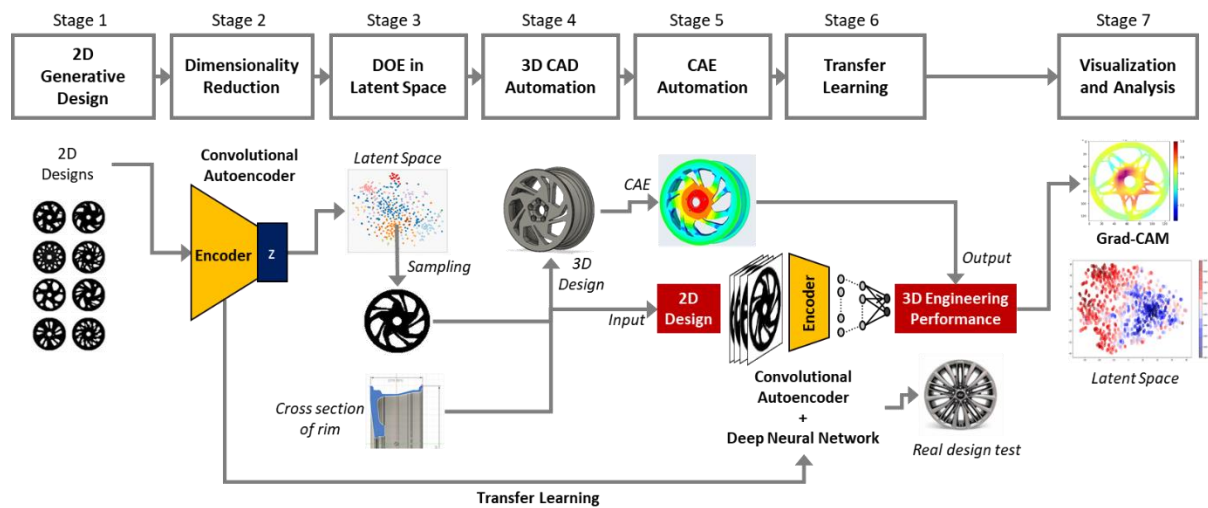


Figure 1. Deep CAD/CAE framework

The deep-learning-based CAD/CAE framework proposed herein comprises seven stages, and the framework is presented in Figure 1. The goals of the framework are summarized as follows: The first goal is to develop a fully automated CAD process that generates 3D CAD data based on 2D generative design by integrating CAD and

CAE through a deep learning process. The second goal is to develop a deep learning model for 3D CAE simulation using only 2D design as input. In the early stages of product development, we can evaluate the engineering feasibility of numerous concept designs using the 2D concept sketch of a designer.

The description of each stage of the proposed framework is presented as follows:

- *Stage 1. 2D generative design:* To generate various 2D wheel designs, we adopted our previous deep generative design process (Oh et al. 2019), which is an effective method combining topology optimization and deep learning to create many engineered structure designs. First, we collected the image data of a commercial wheel as reference designs; subsequently, based on these reference designs, a number of new topology designs of 2D disc-view wheels were generated automatically. In this study, we created 16,689 2D wheel designs, and more details pertaining to Stage 1 are provided in Section 3.
- *Stage 2. Dimensionality reduction:* In this stage, the dimensions of the 2D wheel design generated in Stage 1 are reduced. Dimensionality reduction helps to overcome the curse of dimensionality, thereby allows us to extract important features from 2D wheel designs. In this study, we used a convolutional autoencoder (Masci et al., 2011), which performs well in reducing the dimensionality of images. In our research, 128×128 2D images were mapped into a 128-dimensional latent space. Subsequently, the trained encoder of the convolutional autoencoder was used in Stages 3 and 6. Details of Stage 2 are provided in Section 4.
- *Stage 3. DOE in latent space:* This stage pertains to the DOE process for drawing 2D wheel design samples from the latent space, which are then used for creating CAD data. Because this latent space comprises the feature vectors of the wheel design, the data distribution is more meaningful than the original high-dimensional space. In this study, Latin hypercube sampling (LHS) (Viana, 2018) was used, and 1,030 2D wheel designs were sampled from the latent space. A detailed description of Stage 3 is provided in Section 5.
- *Stage 4. 3D CAD automation:* In this stage, 3D CAD data to be used as input to CAE are automatically generated. First, the 2D wheel design undergoes preprocessing, which involves four steps: (1) smoothing and sharpening of edges, (2) edge extraction, (3) conversion of edges into coordinate data, and (4) grouping of edge coordinates. Next, the process of generating a 3D CAD based on the 2D wheel image and the cross-section image of the given rim is automated. In our study, Autodesk Fusion 360 (Autodesk, 2020) was used to automate 3D CAD modeling. The details of Stage 4 are provided in Section 6.
- *Stage 5. CAE automation:* In this stage, CAE simulation data are collected using the 3D CAD data generated in Stage 4. In this study, we conducted modal analysis to verify the natural frequency of the lateral mode, and the result was stored as labeled data used for deep learning. Altair SimLab (Altair, 2020) was used for CAE automation. The details of Stage 5 are provided in Section 7.
- *Stage 6. Transfer learning:* In this stage, the CAE simulation result of the 3D CAD design is trained by transfer learning. Using the 2D wheel design as input, the deep learning model predicts the natural frequency and mass as the output. In this study, to solve the problem of insufficient data, data augmentation and transfer learning were conducted by combining a DNN with the encoder of a convolutional autoencoder, which was pretrained in Stage 2. Furthermore, we used an ensemble technique to reduce overfitting and improve the prediction performance. Stage 6 is described in detail in Section 8.
- *Stage 7. Visualization and analysis:* In this stage, CAD/CAE engineers can visualize and explain the deep learning results to gain new insights into and evaluate the reliability of the results. The latent space created in Stage 2 can be visualized in two dimensions to examine the relationship between the wheel shape and natural frequency. In addition, the wheel shape that significantly affects the natural frequency can be identified by Grad-CAM. More details regarding Stage 7 are provided in Section 9.

3. 2D Generative Design (Stage 1)

Stage 1 involves creating large amounts of 2D disc-view wheel designs. A part of the deep generative design framework was used in this study, which combined deep learning and topology optimization, as suggested by Oh et al. (2019).

Topology optimization is typically used for structural design, in which a design area is divided into elements and the optimal material density of the elements is determined to minimize compliance considering a given load

and boundary condition. Oh et al. (2019) added a term to the typical topology optimization problem, which minimizes the distance from a reference design to a new topology design. Consequently, the problem becomes a multiobjective problem to obtain a new topology design that is similar to the reference design and has a low compliance simultaneously. The proposed optimization formulation is as follows:

$$\begin{aligned}
\min \quad & f(\mathbf{x}) = \mathbf{U}^T \mathbf{K}(\mathbf{x}) \mathbf{U} + \lambda \|\mathbf{x}_r - \mathbf{x}\|_1 \\
\text{s. t.} \quad & \frac{V(\mathbf{x})}{V_0} = f \\
& \mathbf{K} \mathbf{U} = \mathbf{F} \\
& 0 \leq x_e \leq 1, \quad e = 1, \dots, N_e
\end{aligned} \tag{1}$$

\mathbf{x} is the design variable and is represented by the density vector of the element. \mathbf{U} is the displacement vector, \mathbf{K} is the global stiffness matrix, and $\mathbf{U}^T \mathbf{K}(\mathbf{x}) \mathbf{U}$ corresponds to the compliance. \mathbf{x}_r indicates the reference design, $\|\cdot\|_1$ indicates the L1 norm, and λ is the similarity weight. The larger the λ , the closer the optimal design is to the reference design. For a small λ , the reference design is disregarded, and it is optimized to minimize the compliance. f is the volume fraction, $V(\mathbf{x})$ is the volume of the material, and V_0 is the volume of the design domain. Detailed equations and optimization methods are available in Oh et al. (2019).

In topology optimization, a single optimal design is obtained when the designer defines the objective function, loads, and boundary conditions. Meanwhile, a generative design involves of creating multiple optimal designs by varying the definition of the topology optimization problem. Hence, we define and discretize the design parameters in Eq. (1). Subsequently, Eq. (1) becomes a set of new optimization problems, and the optimal design for each problem can be obtained.

The generative design process is shown in Figure 2. In this study, three design parameters were defined. (1) similarity weights (λ), (2) ratio of normal and shear forces applied outside the wheel, and (3) volume fraction (f). By dividing these values into five levels, we created 125 optimization problems ($5 \times 5 \times 5$) per reference design. For the reference design, 658 real wheel images obtained by web-crawling were preprocessed. The generated wheel designs were filtered again by verifying the similarities; finally, 16,678 new 2D wheel images were obtained, in which the image measured 128×128 .

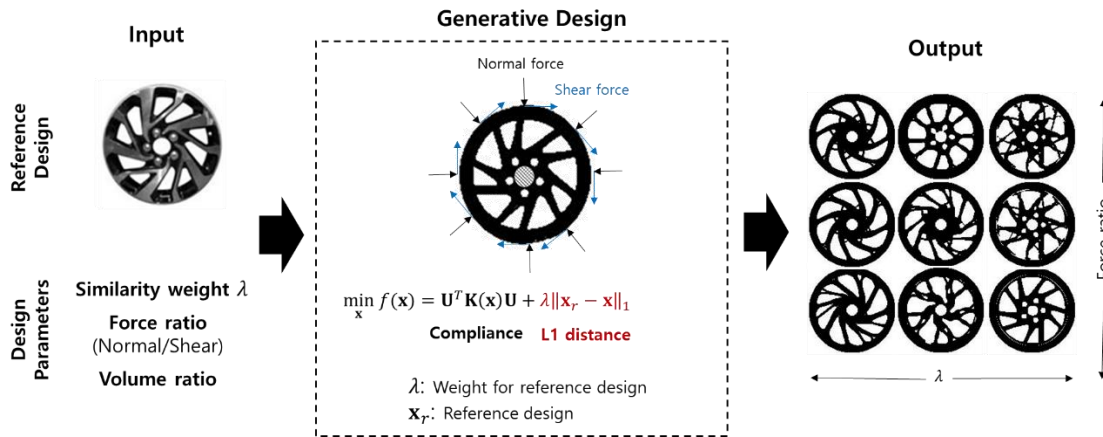


Figure 2. 2D wheel generation by generative design

4. Dimensionality Reduction (Stage 2)

Stage 2 is the process of reducing the dimensions of the 2D wheel design created in Stage 1 using a convolutional autoencoder. Data augmentation was performed to improve the performance, and the latent space was analyzed to verify the feasibility of the trained model.

4.1. Data

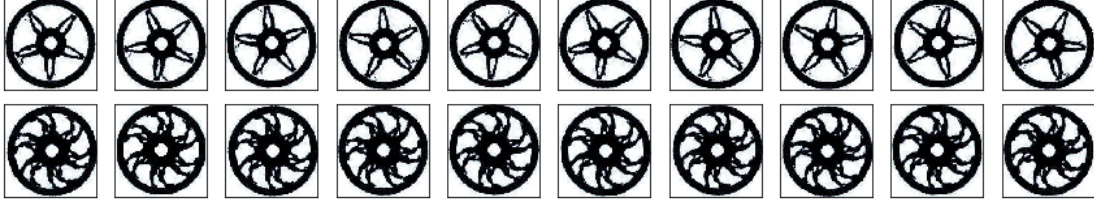


Figure 3. Examples of augmented 2D wheels

Because the wheel is a rotating object, the rotated wheel should not be recognized as a different wheel. Therefore, the data were augmented by rotating randomly in the 360° range. Through this augmentation, the number of 2D wheel design data increased from 16,678 to 166,812 (approximately 10 times larger). Figure 3 shows an example of the rotating the wheel at 10 random angles. This data augmentation resulted in an increase in the training data; hence, the deep learning performance improved.

4.2. Training

The convolutional autoencoder adds convolutional layers to the autoencoder architecture and performs well in the dimensionality reduction of images (Masci et al., 2011). The architecture used is shown in Figure 4.

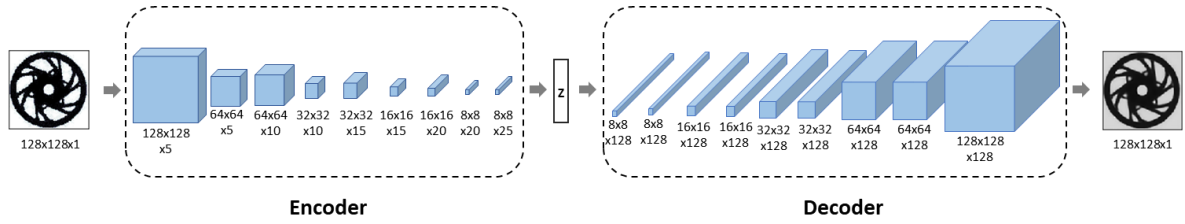


Figure 4. Architecture of convolutional autoencoder

When the 2D wheel image measuring 128×128 as input passed through the encoder part, the dimension was mapped to 128 dimensions in latent space (\mathbf{z}); meanwhile, when the 128 dimensioned values were passed through the decoder again, the 2D wheel image that was the input was reconstructed. If the reduced dimension (128) can reconstruct the original dimensions (128×128), it demonstrates that the 128 dimensions of \mathbf{z} well extracted the important features of the input.

An autoencoder is a model that minimizes the difference values of pixels between an input image and an output image. The autoencoder loss function can be expressed as the mean squared error (MSE) as follows:

$$\text{MSE} = \frac{1}{n} \sum_{i=1}^n (x_i - \hat{x}_i)^2, \quad (2)$$

where x_i is the i -th input data, \hat{x}_i is the output from the autoencoder, and n is the number of input data. In the convolutional autoencoder architecture, the encoder is composed of five convolutional layers and four maxpooling layers, and the decoder is composed of five convolutional layers, four upsamplings, and a 50% dropout; therefore, it becomes a 128×128 image again. A rectified linear unit (ReLU) was used for the activation function of each convolution layer. The Adam optimizer was used with a learning rate of 0.00008, batch size of 64, and epoch of 100. A total of 133,449 data points (80%) were used as the training set, whereas 33,363 data points (20%) were used as the validation set. Figure 5 shows the learning results. The model converged well in both the training and validation sets.

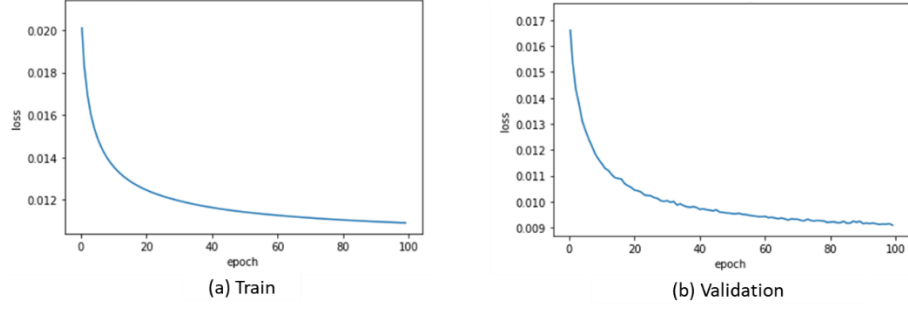


Figure 5. Reconstruction error of convolutional autoencoder

4.3 Testing

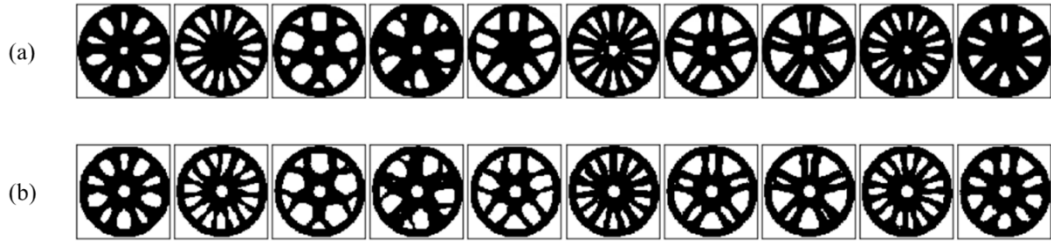


Figure 6. (a) original image (b) reconstructed wheel image in test set

To visually verify whether the model has learned the features well, we reconstructed 96 real wheel images of the manufacturer that were not used for the training and validation. As shown in Figure 6, it was confirmed that the wheels in the test set were reconstructed similarly to the input. Therefore, it can be concluded that the latent space well represented the wheel-shaped features. In addition, in the training set, holes were uniformly drilled in the center of the wheel. Therefore, even if no holes exist in the test data (i.e., the rightmost figure in Figure 6), a hole of the same size is created in the reconstructed wheel. Hence, it can be concluded that the model learned that the center of the wheel is always drilled.

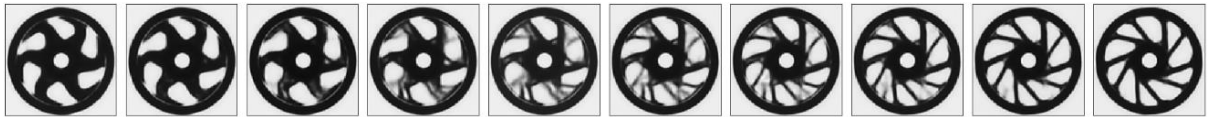


Figure 7. Interpolation result in z latent space

Interpolation is a method to verify whether the deep learning generative model has been well trained for the latent space. When the model only memorizes the input wheel to reconstruct the input wheel, the interpolated wheel image in the latent space does not naturally deform, and the shape of the wheel suddenly changes stepwise. After encoding the two wheels in the training set to two vectors in the latent space, these vectors were divided by the same distance, and 10 vectors were extracted from the latent space. The results of decoding the 10 vectors are shown in Figure 7. Two wheels located on the leftmost and rightmost sides appeared completely different, but the wheels reconstructed from the 10 vectors in latent space changed gradually while maintaining the features of both sides. Therefore, it can be concluded that the convolutional autoencoder has learned the latent space continuously.

5. DOE in latent space (Stage 3)

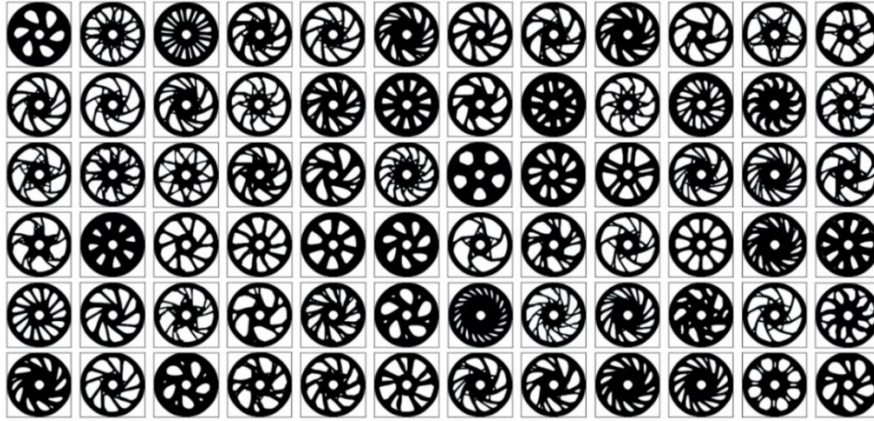


Figure 8. Sampled 2D wheel designs from latent space

LHS from a normal distribution was used to conduct the DOE in the latent space, and the LHSnorm function in MATLAB (Mathworks, 2020) was used. When training data were encoded in the latent space, the data were not distributed uniformly but exhibited a normal distribution. We discovered that a good wheel-shape image can be sampled when we used the LHSnorm and not the LHS. After sampling 3000 vectors from a 128-dimensional multivariate normal distribution with the mean and covariance of the training data in the latent space, the training wheels that were closest to the sampled vectors were selected. The reason for using the nearest training wheel design without using the decoded image was that the main purpose of the convolutional autoencoder was to reduce dimensions, not to generate new images. Finally, we selected 1300 designs after filtering to verify the similarity. Figure 8 shows examples of the sampled wheel design.

6. 3D CAD Automation (Stage 4)

The process of Stage 4, i.e., creating a 3D CAD model from a 2D image, was performed in three steps, as shown in Figure 9. The first step was image processing, which uses anti-aliasing to create smooth and sharp edges of the 2D wheel design samples. The second step was data processing by grouping neighboring points to create splines and centering them. The third step was automatic 3D CAD generation using the Python API of Autodesk Fusion360 (Autodesk, 2020).

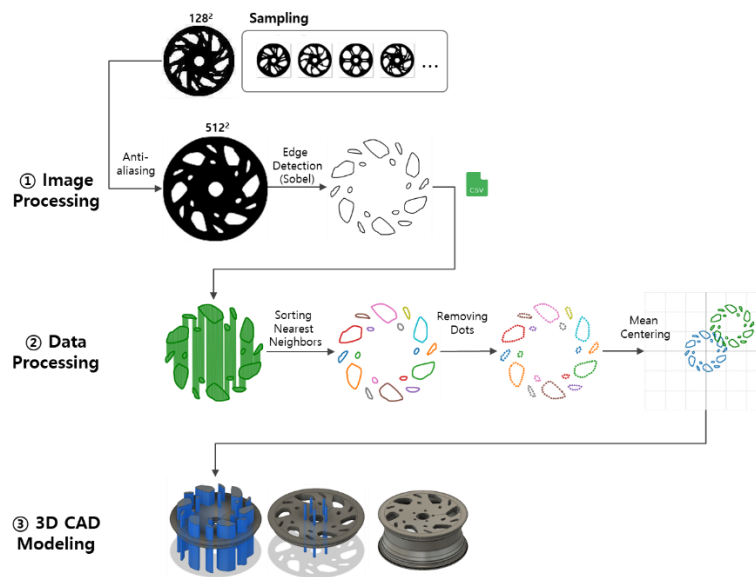


Figure 9. Three steps of Stage 4

6.1. Image Processing

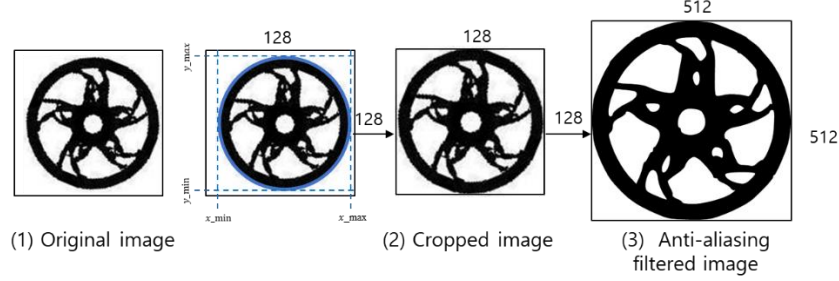


Figure 10. Anti-aliasing filtering

The original image created in Stage 3 contained a margin at the edge. Because the position of the wheel must be the same in all images, the margin must first be removed. Therefore, we detected the edge, obtained the maximum and minimum values of x and y from the detected data, and cropped the image in the range of $[x_{min} \sim x_{max}, y_{min} \sim y_{max}]$ of the original image. Subsequently, we obtained the image with no margin, as shown in Figure 10.

A low-pixel image appeared as a stepped line owing to the large size of the square pixel; this phenomenon is known as aliasing. In our study, the original image comprised 128×128 pixels; therefore, we applied anti-aliasing (AA) (Catmull, 1978) to all the images, which reduced the anti-aliasing by smoothing. AA converts a pixel graphic file to a vector graphic file; therefore, we converted the PNG file into the scalable vector graphics format and then converted it back to a PNG file to obtain an anti-aliased image. In the AA process, a higher pixel image was attainable because more pixels were added to smooth the aliasing portion. Figure 10 shows an example of obtaining a 512×512 high pixel image by applying AA to a 128×128 wheel image.

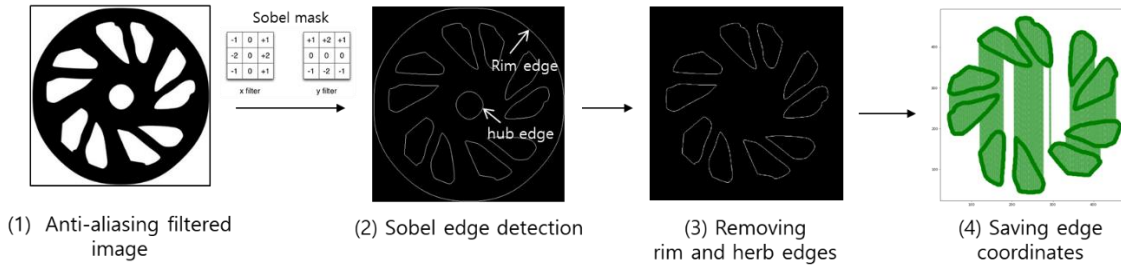


Figure 11. Edge detection

Edge detection involves obtaining the boundaries of objects in an image, where the boundary is an area with a large change rate in brightness. The change rate in brightness is called the gradient; after calculating the gradient in the image, the edge can be determined according to the threshold value. The first derivative, which is an approximation of the difference between adjacent pixels, was performed in the horizontal and vertical directions. The gradient magnitude ∇G is calculated as follows:

$$\nabla G = \sqrt{G_x^2 + G_y^2}, \quad (3)$$

where $G_x = f(x + 1, y) - f(x, y)$

$$G_y = f(x, y + 1) - f(x, y)$$

The horizontal difference is G_x , the vertical difference is G_y , and the brightness function is f .

A representative method of edge extraction using the first derivative is the Sobel operator (Kanopoulos et al., 1988). The Sobel operator can extract diagonal edges well; therefore, it is well suited for edge detection in 2D wheel designs. After extracting the entire edge of the image, the edges of the rim and hub were removed to use

only the edges of the spoke areas. Subsequently, the coordinates of the final edges were saved in a .csv file.

6.2. Data Processing

Data processing was performed to connect the spoke edges with splines for CAD modeling automation. The data are the coordinates of the 2D pixels, which we call coordinates points.

In this study, we first organized the points based on distance and group adjacent points. Figure 12 shows the sorting and grouping process. We calculated the Euclidean distance between one fixed point and another to obtain the shortest distance. This allows the points to be organized by the shortest distance. If the point closest to the fixed point is greater than or equal to the threshold value, it is regarded as a different group.

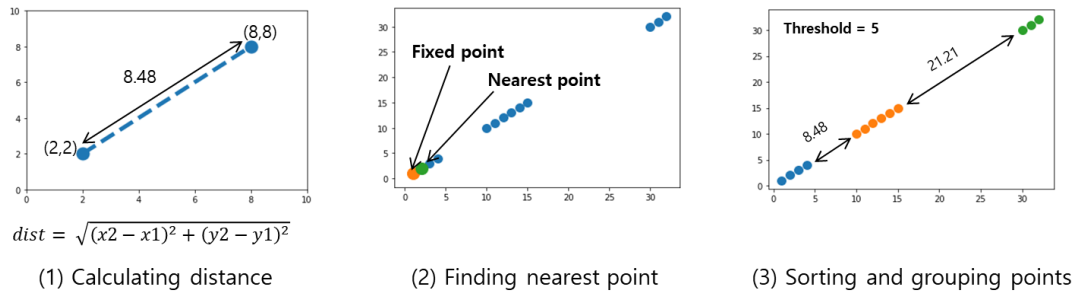


Figure 12. Algorithm for sorting and grouping points

If all the points in each group are used for generating the spline curve, the curve will be tortuous and not smooth. This can misrepresent the original shape and cause errors in the CAD modeling. Therefore, the spline curve of the spoke should be designed using the correct number of points after filtering unnecessary points. This process is shown in Figure 13.

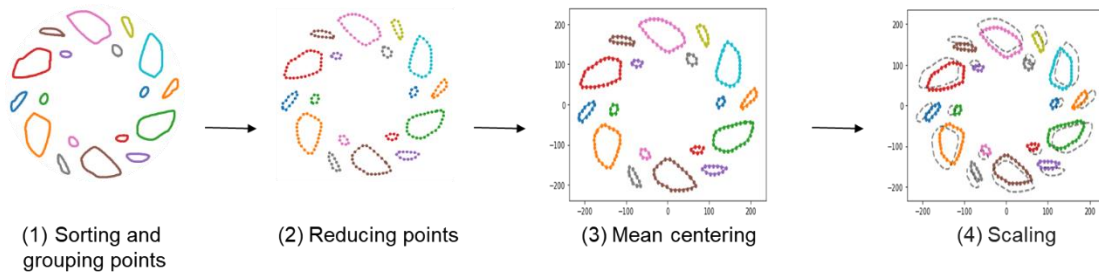


Figure 13. Data processing

In this study, we determined the deletion rate according to the number of points in each group. The group comprising more than 20 points and less than 100 points was reduced to 1/6, whereas that comprising 100 points or more was reduced to 1/12. We did not reduce points in a group comprising less than 20 points. However, if the number of points is 3 or less, it is considered as noise and the group is deleted. Finally, all coordinates were moved to the center of the origin (i.e., mean centering). Subsequently, to design a spoke that fit an 18-inch wheel, each point group was multiplied by a scalar, 0.97.

6.3. 3D CAD Modeling

3D modeling requires not only the disc-view shape, but also the cross-sectional shape of the spokes and rim. The aim of this study is to create wheels with the same cross section and diverse spoke shapes. Typically, in the development of road wheels, the rim cross-section has a limited degree of freedom owing to the packaging

constraints of the parts inside the rim. Therefore, we selected the 18-inch representative wheel model with a rim width of $7.5j$, which is a flagship vehicle. j represents the size of the rim and is indicated in inches. From the selected CAD model, the cross sections of the spoke and rim were extracted, and the coordinates of each point were stored in a .csv file. The stored points were used to automatically design cross-sectional shapes through lines and spline curves in 3D modeling, as shown in Figure 14.

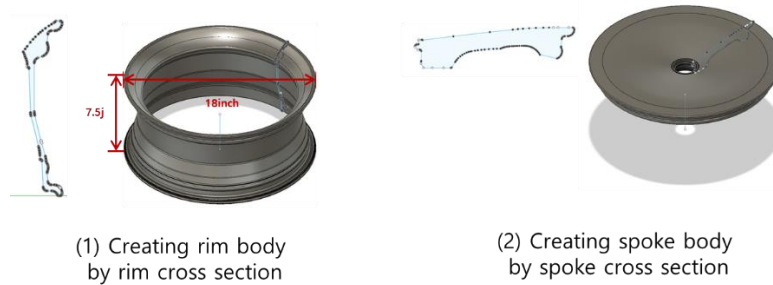


Figure 14. 3D modeling using selected cross-sections of rim and spokes

Figure 15 shows the overall process of 3D CAD modeling using the 2D information of disc-view spoke shape and the cross section obtained in previous steps. This process was fully automated using the Python API of Autodesk's Fusion360. The 2D information was obtained from the .csv file and loaded sequentially in the order specified.

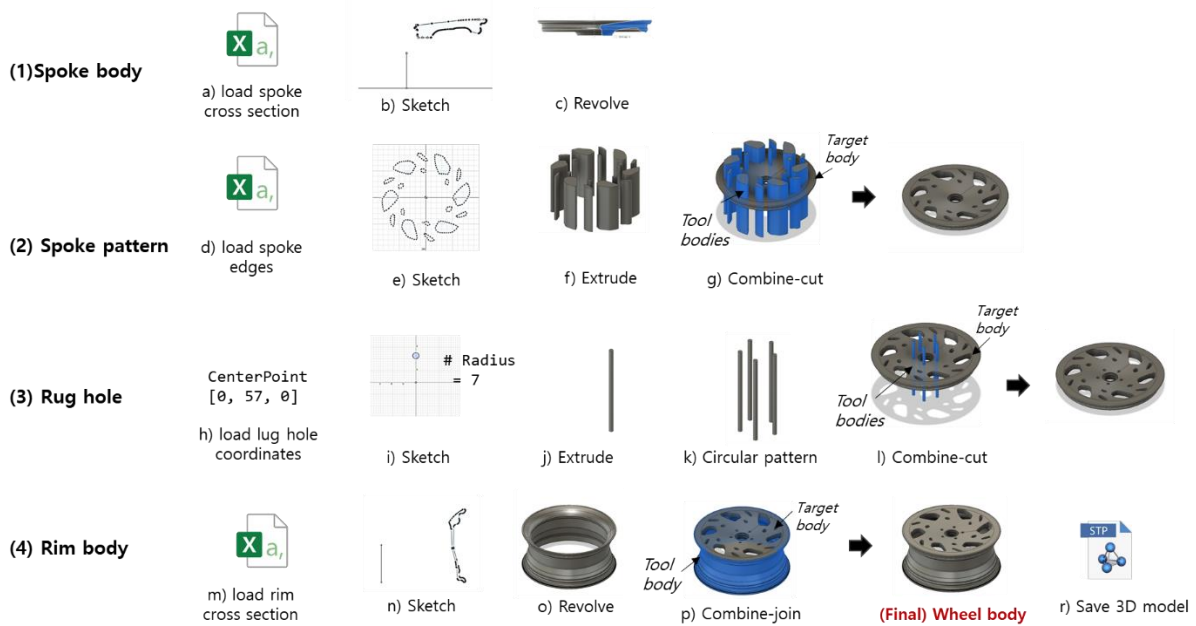


Figure 15. Process of the automatic generation of 3D wheel CAD using given 2D information

The detailed process is as follows:

First, the cross-section of the spoke was sketched by loading the coordinates and connecting the points by lines and splines. When the cross-section was revolved, a spoke body was created.

Second, the disc-view was sketched by loading the coordinates of the spoke edges and connecting the points of each group by a spline. The bodies of the spoke shape were created when sections of the spoke shape were extruded. These spoke-shaped bodies were designated as tool bodies, whereas the spoke body was designated as the target body. Subsequently, a combine-cut was performed to remove the intersection of the two bodies. Consequently, the tool bodies disappeared, and the target body without a cross section remained.

Third, after defining the reference lug hole center coordinates and radius, the circular cross section was sketched and extruded to create a cylindrical body. Subsequently, the same circular column bodies were generated at 72° intervals using the reference body. The five cylindrical bodies created were designated as tool bodies, whereas the spoke body was designated as the target body. A combine-cut was performed to remove the intersection between the bodies, thereby creating lug holes in the spoke body.

Fourth, the cross-section of the rim was sketched by loading the coordinates and connecting the points by the lines and splines. The sketch was then revolved to create a rim body. A combine-join was performed to combine the rim body and spoke body, and then a final wheel body was created. The wheel body was saved in .stp format, which is a universal 3D CAD file format.

Figure 16 shows examples of automatically generated 3D CAD models.

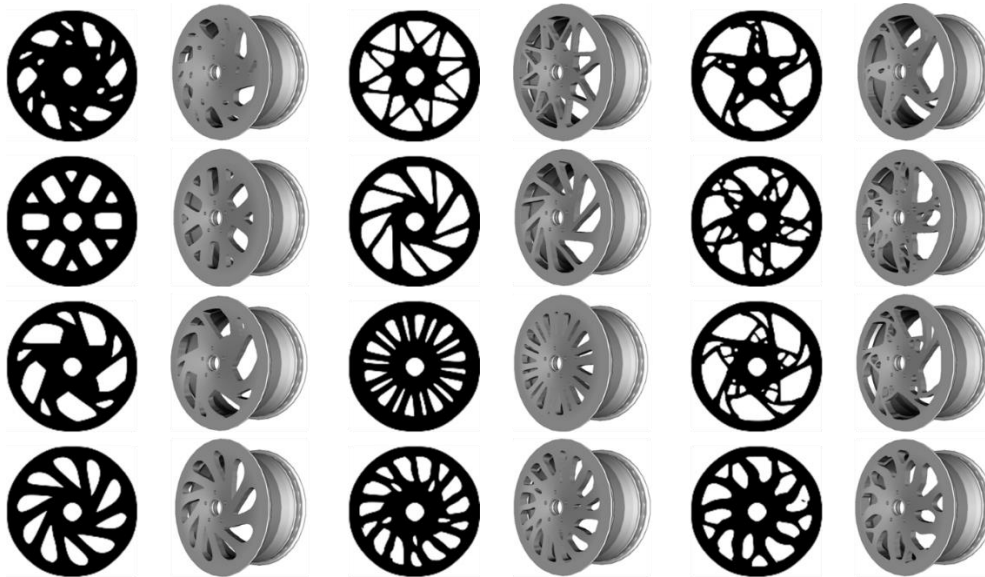


Figure 16. Auto-generated 3D wheel CAD models

7. CAE Automation (Stage 5)

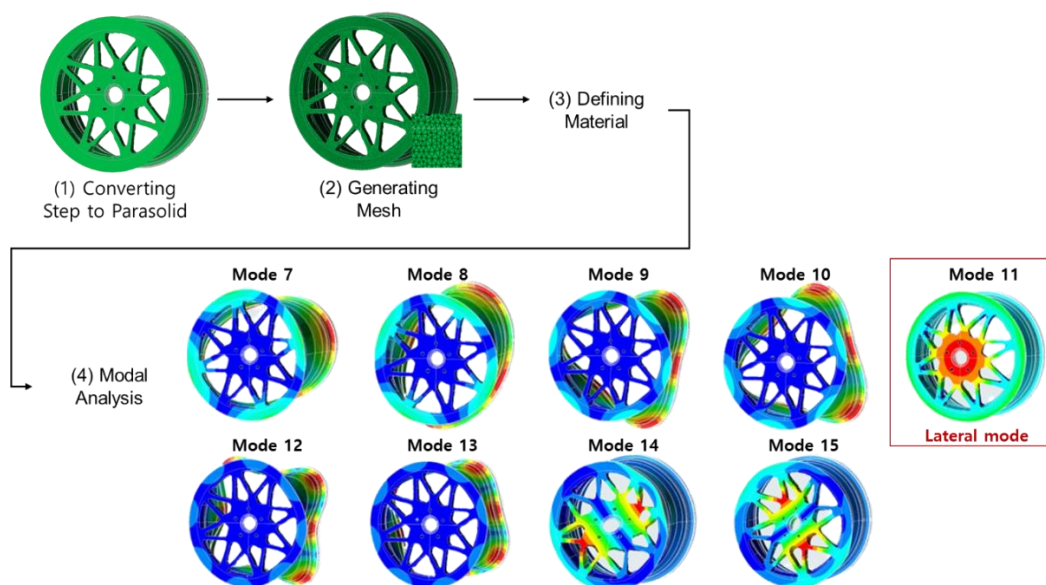


Figure 17. Example of modal analysis and results

In this study, modal analysis was conducted to analyze the engineering performance of the wheel, where the natural frequencies of the structures and the mode shapes at each natural frequency were analyzed. In particular, the natural frequency is proportional to the stiffness of the structure and inversely proportional to mass as follows:

$$f = \frac{1}{2\pi} \sqrt{\frac{k}{m}}, \quad (4)$$

where f is the natural frequency, k the stiffness, and m the mass. Therefore, when designing a wheel, manufacturers consider a lower bound of stiffness for each mode as a design constraint, based on the correlation between the stiffness for each mode and road noise.

We conducted a free-free modal analysis. The unconstrained 3D model contained six rigid body modes with zero frequency, three translation modes in the x- and y-axis directions and three rotation modes for the three axes. Beginning from the seventh mode, a nonzero frequency appeared. For the wheel, modes 7 and 8, modes 9 and 10, mode 11, modes 12 and 13, and modes 14 and 15 indicate rim mode 1, rim mode 2, the spoke lateral mode, rim mode 3, and the spoke bending mode, respectively, as shown in Figure 17. The frequency for the lateral mode (mode 11) was selected in this study because we intended to evaluate the engineering performance according to the shape of the spoke. In addition, after the mass has been obtained from the 3D modeling, the stiffness can be calculated through the natural frequency and mass using Eq. (4).

For CAE automation, the macro function in Altair's Simlab (Altair, 2020) was used. The modal analysis process is shown in Figure 17. First, the 3D CAD model was imported; next, an FEM mesh (second-order tetrahedral mesh) was automatically generated. The size of the mesh should not be larger than 6 mm. We used the material properties of the reference aluminum wheels, from which the rim cross-section was extracted. Finally, when the analysis was completed, the result was saved as a text file.

The CAE automation yielded 1006 output files, which was also the number of input 3D CAD files. To automatically extract the necessary information from the output text file, we coded a parsing program that read the text file line by line, obtained the index of the string containing the required values, and then extracted the required values and saved them as a .csv file. This was because the input 2D wheel image, frequency (mode 11), and mass were stored in pairs as training data for deep learning.

8. Transfer Learning (Stage 6)

In Stage 6, deep learning was developed, in which the results of modal analysis and the mass of the 3D CAD model were predicted using only 2D design. Data augmentation and data scaling were performed as data preprocessing; furthermore, transfer learning and ensemble techniques, in which the pretrained convolutional autoencoder and DNN were combined, were applied to solve the problem of insufficient data.

8.1. Data

Data augmentation was performed to avoid overfitting. We augmented the 1006 wheel designs that we sampled in Stage 3 10 times, rotating each of them by 72° and flipping them left and right. Consequently, 10,060 datasets were used for training. The output values were equivalent because imposing the left and right flips did not affect the modal analysis and mass result.

Furthermore, 80% of the 10,060 data was used as the training set, and the other 20% was used for validation. Although a new design that does not exist in the market because it was created with a generative design was used for training and validation, 96 wheel images was used for the test set, which were sold by the manufacturer. This was to confirm whether the trained model can predict the actual data of the manufacturer. The frequency and mass values of the test set were obtained through Stages 4 and 5, respectively, identical to the training data.

In addition, we used min-max scaling, which was adjusted to a fixed range (regularly 0 to 1) for the output labels. The formula for y_{scale} is as follows:

$$y_{scale} = \frac{y - y_{min}}{y_{max} - y_{min}} \quad (5)$$

8.2. Training

In this study, to obtain the optimal architecture and assess the degree to which transfer learning and ensemble affects performance, we trained four models that corresponded to Table 1.

Table 1 Four deep learning architectures

Models	Description
CNN	A model that uses only a CNN regressor and not transfer learning (added seven fully connected floors, four max pooling layers, and five convolution layers, i.e., the same structure as the encoder part of the convolutional autoencoder).
TL_VGG16	A model that uses transfer learning through a pretrained VGG16 (using ImageNet dataset).
TL_CAE	A model that uses transfer learning through the pretrained convolutional autoencoder model (see Figure 18).
TL_CAE_Ensemble	A model that applies ensemble in TL_CAE and trains using the averaging technique for nine frequency models and five mass models (see Figure 19).

First, the CNN was used as a baseline model.

Second, TL_VGG16 is a model that uses a trained VGG16 (Simonyan and Zisserman, 2014) as transfer learning. Transfer learning transfers the pretrained deep learning model from the domain where data are abundant, which is a method to train a domain that lacks data; moreover, it is one of the most used methodologies in deep learning because it can accomplish a high accuracy despite insufficient data. (Rawat and Wang, 2017)

Third, TL_CAE is a representative model used in this study, which transfers the weight and architecture of the encoder of the convolutional autoencoder model pretrained using 166,812 data in Stage 2, adds fully connected layers as a regressor, and performs fine-tuning using 10,060 data from the modal analysis result. Figure 18 shows a visualization of the deep learning architecture used in this study. Although we performed an augmentation (as mentioned in Section 8.1), the number of modal analysis results (label) was 1,006, which was small but expected to improve the performance using the encoder pretrained using 166,812 data (a large amount). The newly added regressor part comprised seven fully connected layers. It was trained using the Adam optimizer, in which the learning rate was 0.002, decay rate was 0.001, and batch size was 256. Early stopping was applied.

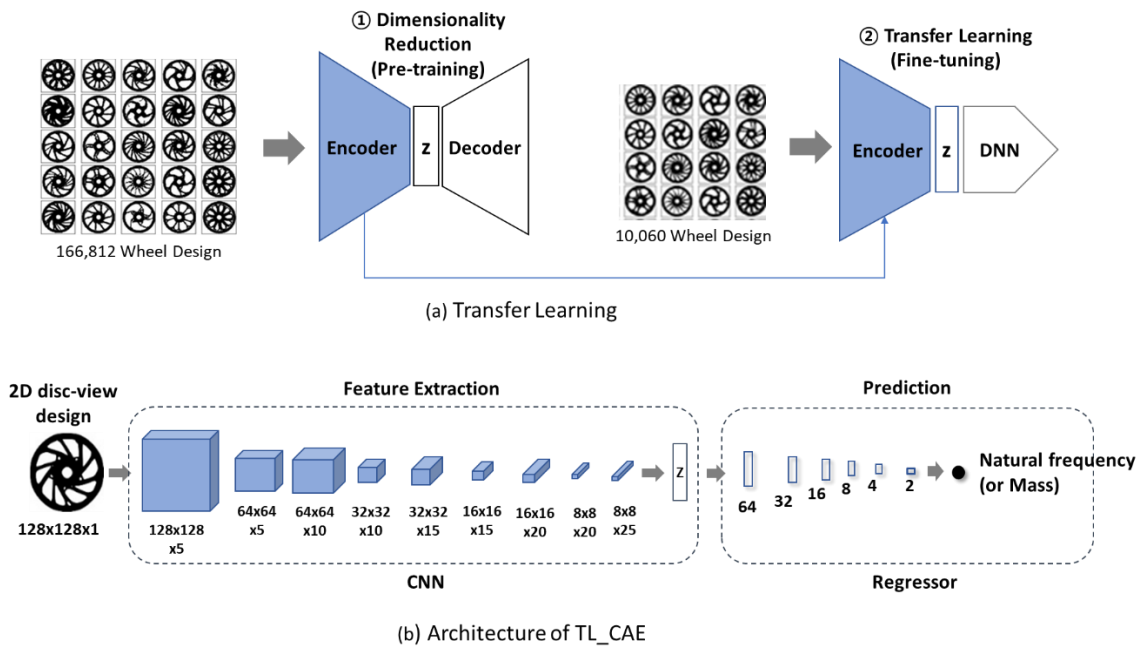


Figure 18. Transfer learning using convolutional autoencoder (TL_CAE)

Fourth, the final model TL_CAE_Ensemble was built using the ensemble technique, as shown in Figure 19. The ensemble technique offers the advantage of avoiding overfitting in regression problems and reducing bias deviation (Geurt et al., 2006). It is a method of standardizing the prediction results by assembling multiple models into a single model. Our ensemble model uses the mean values of nine frequency prediction results and five mass prediction results. For the frequency prediction model, the training required 15 min on four GPUs (GTX 1080) in parallel.

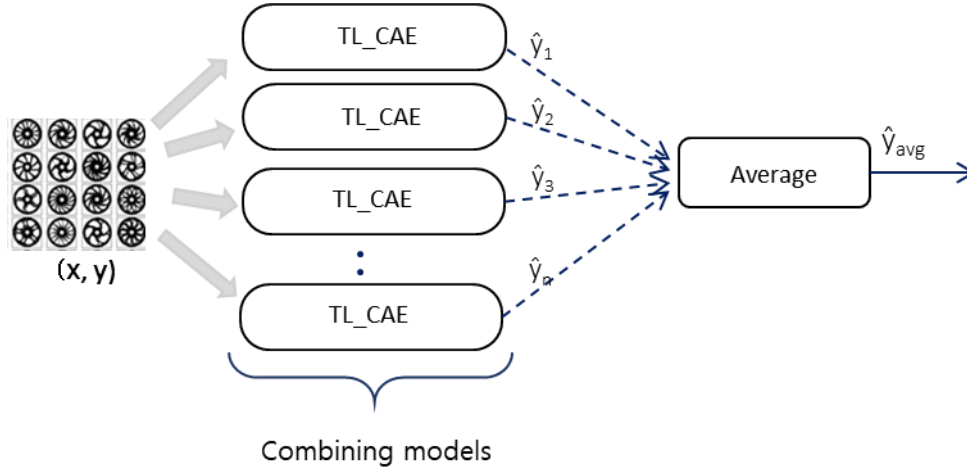


Figure 19. Ensemble model for TL_CAE (TL_CAE_Ensemble)

8.3. Testing

To evaluate the performance of the prediction model, two metrics, the root mean square error (RMSE) and the mean absolute percent error (MAPE) were used. They are expressed as follows:

$$RMSE = \sqrt{\frac{1}{n} \sum_{i=1}^n (\hat{y}_i - y_i)^2} \quad (6)$$

$$MAPE = \frac{100}{n} \sum_{i=1}^n \left| \frac{\hat{y}_i - y_i}{y_i} \right| \quad (7)$$

\hat{y} is the predictive value, y the ground truth value, and n the number of data points. The performance results of the four trained models are shown in Table 2. TL_CAE indicated improved RMSE and MAPE compared with TL_VGG16. This result confirmed that the proposed convolutional-autoencoder-based transfer learning performed effectively. In addition, the final model, TL_CAE_Ensemble, demonstrated the best predictive performance in terms of both the RMSE and MAPE.

The errors for the validation and test sets of the three models are represented as histograms, as shown in Figure 20. The closer the error is to 0, the higher is the accuracy of the model. These results confirmed the effects of transfer learning and the ensembles.

Table 2 Comparison of frequency and mass prediction results

Method	* units: Frequency (Hz), Mass (kg)											
	Training set				Validation set				Test set			
	Frequency RMSE	MAPE	Mass RMSE	MAPE	Frequency RMSE	MAPE	Mass RMSE	MAPE	Frequency RMSE	MAPE	Mass RMSE	MAPE
CNN	13.0	1.06	0.10	0.48	16.71	1.24	0.09	0.44	20.97	3.51	0.33	1.89
TL_VGG16	4.58	0.36	0.26	1.46	6.57	0.50	0.27	1.49	20.56	1.74	0.19	0.91
TL_CAE	8.89	0.69	0.09	0.44	10.44	0.82	0.09	0.45	18.89	1.38	0.13	0.67
TL_CAE Ensemble	7.35	0.56	0.06	0.28	8.72	0.66	0.06	0.29	12.78	0.90	0.12	0.54

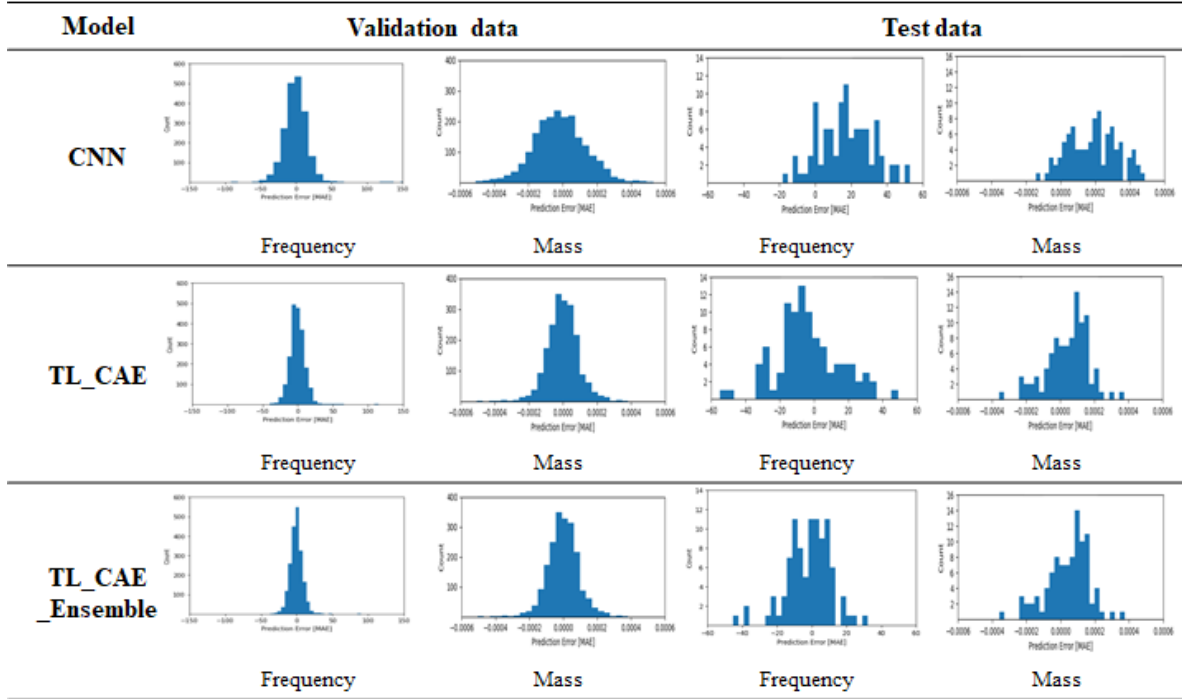


Figure 20. Comparison of errors

9. Visualization and Analysis (Stage 7)

This section describes the visualization and deep learning results from using the proposed framework, and the approach to ensure the reliability of the results.

9.1. Feature Visualization

We visualized the latent space of the convolutional autoencoder in Stage 2 to analyze the explainable features of the generated wheel shape. We embedded 16,678 wheel data into the 128 dimensions of the latent space, and then grouped the data by K-means clustering. In the K-means method, the sum of squared errors (SSE) was plotted over the number of clusters. Additionally, the value corresponding to the elbow, which is the part where the SSE reduction rate decreased rapidly, was determined as the number of clusters. Because the shape of the wheel varied significantly, a large number of groups was required. However, we arbitrarily set the number of clusters to 20 because an excessive number would complicate intuitive analyses by CAD/CAE engineers. In Figure 21, for the visualization, the latent space of 128 dimensions was reduced to two dimensions again through T-SNE (Maaten & Hinton, 2008) to display the data, and the colors of the 20 groups are displayed. In addition, the example wheels of each group were selected and shown.

Commercially available road wheels can be classified into the dish, spoke, mesh, fin, and spiral types according to the shape (Napac, 2020); furthermore, these types can be compounded on one wheel. In this study, the spiral type is the most typically generated. This is because shear force was applied to generative design. In addition, in terms of spoke thickness, groups 4, 7, 12, 16, 17, and 19 were relatively thin, whereas groups 6, 11, 13, and 15 were relatively thick. This visualization of latent space facilitates the understanding of the geometric meaning of positions in a latent space.

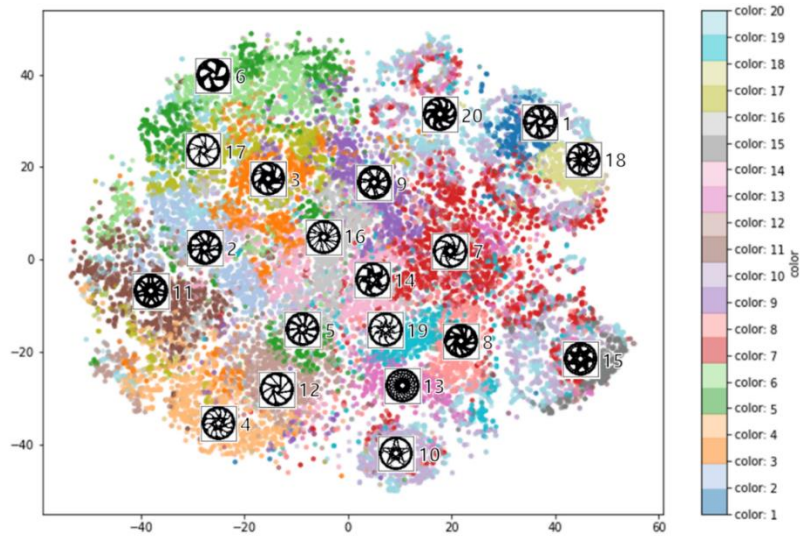


Figure 21. Visualization of latent space using T-SNE

9.2. Relationship Between Features and Engineering Performance

As shown in Figure 22, visualization was performed to determine if the modal analysis result, which is the engineering performance, can be explained by the features of the wheel shape. We embedded 1006 wheels that were used in the modal analysis in Stage 5 into the latent space and visualized them in a two-dimensional plane using T-SNE. In addition, the magnitude of the natural frequency value of each wheel is displayed in color. The frequency value was categorized into 10 groups using K-means. Higher frequencies are represented in red, whereas lower ones, in blue.

Figure 22 shows that wheels with similar natural frequencies accumulated in the latent space, which represents the wheel shape. It was confirmed that the disc-view shape of the wheel was highly correlated with the lateral mode frequency. As shown in Figure 23, we sampled example wheels from each frequency group; the results shows that the thicker the spoke, the more the frequency increases.

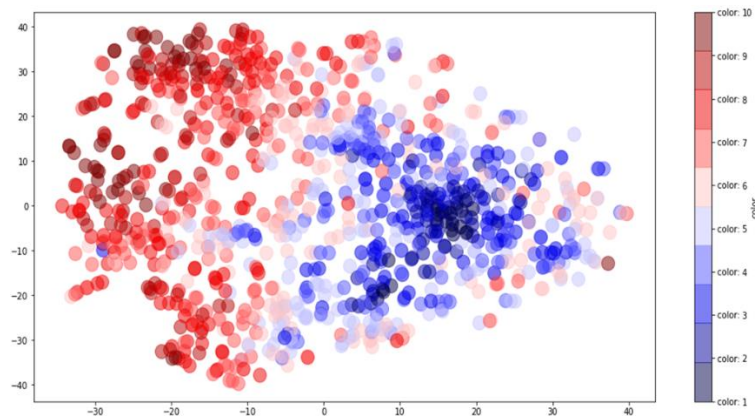


Figure 22. Visualization of latent space with lateral mode frequency































Group	1	2	3	4	5	6	7	8	9	10
Frequency	736-797	802-863	864-910	911-949	949-986	987-1025	1025-1066	1068-1111	1112-1156	1157-1221
Wheel										
										
										

Figure 23. Wheel design of each lateral mode frequency group

This visualization enables clusters of high-performance designs to be selected and important design features to be analyzed intuitively. Furthermore, it provides a method to visually verify the reliability of CAD/CAE results and gain insights into better performance designs.

9.3. Grad-CAM

The high predictive performances afforded by AI are difficult to explain. Hence, the importance of eXplainable AI (XAI) research is increasing. A representative XAI technology, Grad-CAM (Selvaraju et al., 2017), was applied to the proposed framework, allowing CAD/CAE engineers to make reliable decisions based on deep learning results.

A class activation map (CAM) can be used to visualize important areas of input data (images) that significantly affect the classification output in the CNN model (Zhou et al., 2016). A CAM is obtained by adding global average pooling (GAP), a FC layer, and softmax to the feature map, which is the output of the last convolutional layer. The weight of the FC layer indicates the importance of each feature map to the target class label. After multiplying each feature map by weights and adding them together, we can obtain a CAM that can be visualized using a heat map. The disadvantage of the CAM is that GAP must be added to the CNN architecture and then the model must be trained again. However, Grad-CAM does not require the CNN architecture to be modified. This is because Grad-CAM uses gradients obtained through backpropagation instead of using the weights of the FC layer.

Originally, Grad-CAM was proposed for the classification problem; however, we modified it in our study to adapt to the regression problem. The equation of the regression score $L_{Grad-CAM}$ is as follows:

$$L_{Grad-CAM} = ReLU(\sum_k a_k A^k), \quad (8)$$

$$\text{where } a_k = \frac{1}{z} \sum_i \sum_j \frac{\partial y}{\partial A_{ij}^k}$$

A_{ij}^k indicates the value corresponding to i rows and j columns of the k -th feature map, and a_k is the GAP result of the partial derivative of y by A_{ij}^k . After linearly combining a_k with the feature map A^k , the ReLU activation function was applied to obtain Grad-CAM, which can highlight important areas in the image.

Figure 24 shows the visualization result by applying Grad-CAM to the TL_CAE model. Ten example wheels were selected from the 10 frequency groups shown in Figure 23, and the Grad-CAM for each wheel is displayed as a heatmap in the third row of Figure 24. In the second row of Figure 24, the superimposed image shows the common area of the 2D wheel and the Grad-CAM. The results indicate that an important area (highlighted in red) that affected the frequency value was the central part of the wheel. It appeared that the frequency increased as the center was filled. This is because the largest displacement occurred in the center of the wheel in the lateral mode shape (see Figure 17). Therefore, Grad-CAM confirmed that deep learning results can explain the physics of the lateral mode shape and ensure high reliability predictions.

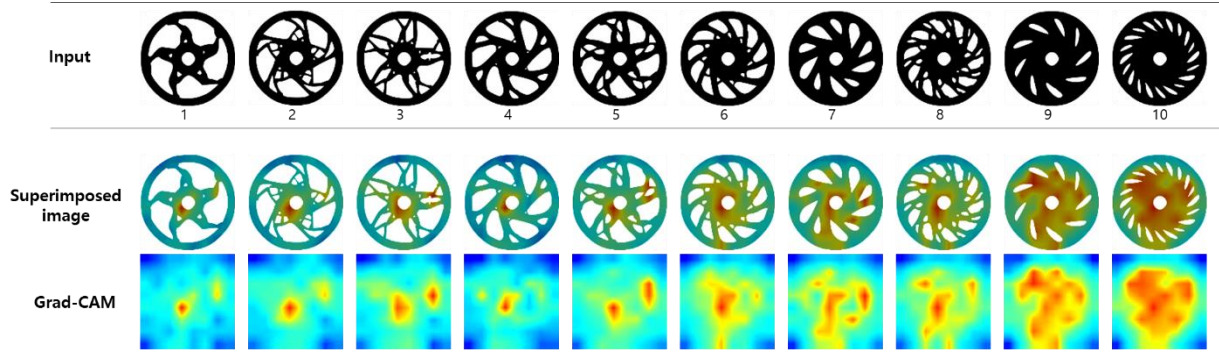


Figure 24. Result of Grad-CAM for frequency of lateral mode

10. Conclusion

A deep learning-based CAD/CAE framework was proposed herein that comprised seven stages: (1) 2D generated design, (2) dimensionality reduction, (3) DOE in latent space, (4) CAD automation, (5) CAE automation, (6) transfer learning, and (7) visualization and analysis. The proposed framework was demonstrated through a case study pertaining to road wheel design, and a practical approach for integrating deep learning and the existing CAD/CAE process was suggested. Using the proposed framework, in the concept design phase of product development, industrial designers and engineers can review large numbers of 3D CAD models created and verified by AI, as well as select the best design.

The contributions of this study are summarized as follows. First, an AI-based CAD automation method was proposed, which enabled 3D wheel CAD data to be generated in large quantities using a 2D generative design. Hence, a solution to the difficulty in obtaining 3D CAD training data for deep learning was obtained. Second, an AI-based CAE performance prediction method was proposed, which enabled the CAE result of the 3D CAD model to be predicted using only a 2D design. In this regard, we automated the CAE process and employed dimensionality reduction, transfer learning, and ensemble techniques for a high prediction performance. Third, AI prediction results were explained through visualization. Using Grad-CAM and dimensionality reduction, CAD/CAE engineers were able to understand the relationship between geometry and engineering performance, thereby enabling them to make reliable decisions.

The future research plan is as follows. First, deep learning will be applied using 3D data as input through the preprocessing of voxels and point clouds. Second, deep learning will be applied to predict nonlinear and dynamic analysis results. Third, a 3D CAD generation method with improved aesthetics will be provided.

Acknowledgements

This work was supported by Hyundai Motor Company and the National Research Foundation of Korea (NRF) grants funded by the Korean government [grant numbers 2017R1C1B2005266, 2018R1A5A7025409]. The authors would like to thank Hyundai Motor Company's Jiun Lee, Sangmin Lee, Min Kyoo Kang, ChangGon Kim, and ChulWoo Jung for their valuable feedback and ideas on our research. We would also like to thank Altair Korea's Jeongsun Lee and Seung-hoon Lee for their help in automating the CAE process.

References

- Altair SimLab. (2019). Retrieved from <https://www.altair.com/>.
- Andreassen, E., Clausen, A., Schevenels, M., Lazarov, B. S., & Sigmund, O. (2011). Efficient topology optimization in MATLAB using 88 lines of code. *Structural and Multidisciplinary Optimization*, 43(1), 1-16.
- Autodesk. (2019). Retrieved from <https://www.autodesk.com/>.
- Burnap, A., Liu, Y., Pan, Y., Lee, H., Gonzalez, R., & Papalambros, P. Y. (2016, August). Estimating and exploring the product form design space using deep generative models. In ASME 2016.
- Cheng, M., Fang, F., Pain, C. C., & Navon, I. M. (2020). Data-driven modelling of nonlinear spatio-temporal fluid flows using a deep convolutional generative adversarial network. *Computer Methods in Applied Mechanics and Engineering*, 365, 113000.
- Cunningham, J. D., Simpson, T. W., & Tucker, C. S. (2019). An investigation of surrogate models for efficient performance-based decoding of 3D point clouds. *Journal of Mechanical Design*, 141(12).
- Edwin Catmull. (1978). "A hidden-surface algorithm with anti-aliasing." In *Proceedings of the 5th annual conference on Computer graphics and interactive techniques (SIGGRAPH '78)*.
- Feng, Y., Feng, Y., You, H., Zhao, X., & Gao, Y. (2019, July). MeshNet: mesh neural network for 3D shape representation. In *Proceedings of the AAAI Conference on Artificial Intelligence (Vol. 33, pp. 8279-8286)*.
- Geurts, P., Ernst, D., & Wehenkel, L. (2006). Extremely randomized trees. *Machine learning*, 63(1), 3-42.
- Guo, X., Li, W., & Iorio, F. (2016, August). Convolutional neural networks for steady flow approximation. In *Proceedings of the 22nd ACM SIGKDD International Conference on Knowledge Discovery and Data Mining (pp. 481-490)*. ACM
- International Design Engineering Technical Conferences and Computers and Information in Engineering Conference (pp. V02AT03A013-V02AT03A013). American Society of Mechanical Engineers
- Kanezaki, A., Matsushita, Y., & Nishida, Y. (2018). Rotationnet: Joint object categorization and pose estimation using multiviews from unsupervised viewpoints. In *Proceedings of the IEEE Conference on Computer Vision and Pattern Recognition (pp. 5010-5019)*.
- Kanopoulos, N., Vasanthavada, N., & Baker, R. L. (1988). Design of an image edge detection filter using the Sobel operator. *IEEE Journal of solid-state circuits*, 23(2), 358-367.
- Khadilkar, A., Wang, J., & Rai, R. (2019). Deep learning-based stress prediction for bottom-up SLA 3D printing process. *The International Journal of Advanced Manufacturing Technology*, 102(5-8), 2555-2569
- LeCun, Y., Bengio, Y., & Hinton, G. (2015). Deep learning. *Nature*, 521(7553), 436-444.
- Li, X., Ning, S., Liu, Z., Yan, Z., Luo, C., & Zhuang, Z. (2020). Designing phononic crystal with anticipated band gap through a deep learning based data-driven method. *Computer Methods in Applied Mechanics and Engineering*, 361, 112737.
- Maaten, L. V. D., & Hinton, G. (2008). Visualizing data using t-SNE. *Journal of Machine Learning Research*, 9, 2579-2605.
- Masci, J., Meier, U., Cireşan, D., & Schmidhuber, J. (2011, June). Stacked convolutional auto-encoders for hierarchical feature extraction. In *International Conference on Artificial Neural Networks (pp. 52-59)*. Springer, Berlin, Heidelberg.
- Matejka, J., Glueck, M., Bradner, E., Hashemi, A., Grossman, T., & Fitzmaurice, G. (2018, April). Dream lens: Exploration and visualization of large-scale generative design datasets. In *Proceedings of the 2018 CHI Conference on Human Factors in Computing Systems (pp. 1-12)*.
- Mathworks [Computer software]. (2020). Retrieved from <https://mathworks.com/>.
- Maturana, D., & Scherer, S. (2015, September). Voxnet: A 3d convolutional neural network for real-time object recognition. In *2015 IEEE/RSJ International Conference on Intelligent Robots and Systems (IROS) (pp. 922-928)*. IEEE.
- Napac. (n.d.). Light Alloy Wheel Categorization by Design. Retrieved from <https://www.napac.jp/cms/en/wheel-words/wheel-design-types>.

- Nie, Z., Jiang, H., & Kara, L. B. (2020). Stress field prediction in cantilevered structures using convolutional neural networks. *Journal of Computing and Information Science in Engineering*, 20(1), 011002.
- Oh, S., Jung, Y., Kim, S., Lee, I., & Kang, N. (2019). Deep generative design: Integration of topology optimization and generative models. *Journal of Mechanical Design*, 141(11).
- Oh, S., Jung, Y., Lee, I., & Kang, N. (2018). Design automation by integrating generative adversarial networks and topology optimization. In *ASME 2018 International Design Engineering Technical Conferences and Computers and Information in Engineering Conference*. American Society of Mechanical Engineers Digital Collection.
- Qi, C. R., Su, H., Mo, K., & Guibas, L. J. (2017). Pointnet: Deep learning on point sets for 3d classification and segmentation. In *Proceedings of the IEEE Conference on Computer Vision and Pattern Recognition* (pp. 652-660).
- Rawat, W., & Wang, Z. (2017). Deep convolutional neural networks for image classification: A comprehensive review. *Neural computation*, 29(9), 2352-2449.
- Selvaraju, R. R., Cogswell, M., Das, A., Vedantam, R., Parikh, D., & Batra, D. (2017). Grad-cam: Visual explanations from deep networks via gradient-based localization. In *Proceedings of the IEEE international conference on computer vision* (pp. 618-626).
- Simonyan, K., & Zisserman, A. (2014). Very deep convolutional networks for large-scale image recognition. *arXiv preprint arXiv:1409.1556*.
- Su, H., Maji, S., Kalogerakis, E., & Learned-Miller, E. (2015). Multi-view convolutional neural networks for 3d shape recognition. In *Proceedings of the IEEE international conference on computer vision* (pp. 945-953).
- Sun, L., Gao, H., Pan, S., & Wang, J. X. (2020). Surrogate modeling for fluid flows based on physics-constrained deep learning without simulation data. *Computer Methods in Applied Mechanics and Engineering*, 361, 112732.
- Umetani, N. (2017, November). Exploring generative 3D shapes using autoencoder networks. In *SIGGRAPH Asia 2017 Technical Briefs* (p. 24). ACM.
- Umetani, N., & Bickel, B. (2018). Learning three-dimensional flow for interactive aerodynamic design. *ACM Transactions on Graphics (TOG)*, 37(4), 89.
- Wang, H., Zeng, Y., Li, E., Huang, G., Gao, G., & Li, G. (2016). "Seen Is Solution" a CAD/CAE integrated parallel reanalysis design system. *Computer Methods in Applied Mechanics and Engineering*, 299, 187-214.
- Williams, G., Meisel, N. A., Simpson, T. W., & McComb, C. (2019). Design repository effectiveness for 3D convolutional neural networks: application to additive manufacturing (DETC2019-97535). *Journal of Mechanical Design*, 1-44.
- Zhang, Z., Jaiswal, P., & Rai, R. (2018). FeatureNet: Machining feature recognition based on 3D Convolution Neural Network. *Computer-Aided Design*, 101, 12-22.
- Zhou, B., Khosla, A., Lapedriza, A., Oliva, A., & Torralba, A. (2016). Learning deep features for discriminative localization. In *Proceedings of the IEEE conference on computer vision and pattern recognition* (pp. 2921-2929).